Measurement report: Atmospheric mercury in a coastal city of Southeast China: inter-annual variations and influencing factors

Jiayan Shi[1,2,4], Yuping Chen[1,2,3], Lingling Xu[1,2,*], Youwei Hong[1,2], Mengren Li[1,2], Xiaolong Fan[1,2], Liqian Yin[1,2],Yanting Chen[1,2], Chen Yang[1,2,3], Gaojie Chen[1,2,3], Taotao Liu[1,2,3], Xiaoting Ji[1,2,3], Jinsheng Chen[1,2,*]

[1] Center for Excellence in Regional Atmospheric Environment, Institute of Urban Environment, Chinese Academy of Sciences, Xiamen 361021, China

[2] Key Lab of Urban Environment and Health, Institute of Urban Environment, Chinese Academy of Sciences, Xiamen 361021, China

[3] University of Chinese Academy Sciences, Beijing 100049, China

[4] College of Resources and Environment, Fujian Agriculture and Forestry University, Fuzhou 350002, China

Correspondence: Lingling Xu (linglingxu@iue.ac.cn) and Jinsheng Chen (jschen@iue.ac.cn)

Abstract. Long-term monitoring of atmospheric mercury is an important part of the effective evaluation of the Minamata Convention on Mercury. Gaseous elemental mercury (GEM) along with conventional air pollutants and meteorological parameters were simultaneously observed in Xiamen city, Southeast China in January and July over the period 2012 – 2020. GEM concentrations in January highest in 2015 (4.47 ng m^{-3}) and decreased to 2020 (3.93 ng m^{-3}), while GEM concentrations in July were highest in 2017 (2.65 ng m^{-3}) and lowest in 2020 (1.56 ng m^{-3}). The temporal variation of GEM was typically characterized by higher concentrations in winter than in summer and in nighttime than in daytime. Bivariate polar plots and Concentrations-weighted trajectories (CWT) model were used to identify the source regions of GEM on a local and regional scale. The results indicate that the high GEM concentrations in January 2015 were likely due to a combination of high-level Hg emissions and adverse meteorological conditions. Generalized Additive Models (GAMs), a regression analysis method, were established and applied to investigate the influencing factors on the inter-annual variation of GEM. The factors, anthropogenic emissions, meteorological conditions and transportation explained 37.8 ± 11.9%, 31.4 ± 9.0% and 30.8 ± 9.9% in average to the variation of GEM concentrations, respectively. There was a positive relationship of daily GEM concentrations with T and RH, mostly linking to natural surface emissions and Hg chemical transformations. The interpretation rate of anthropogenic emissions has significantly decreased since 2012, indicating the effectiveness of emission mitigation measures in reducing GEM concentrations in the study region.

Keywords: Inter-annual variation; Gaseous elemental mercury; GAMs; CWT analysis; Meteorology factors.

1 Introduction

Atmospheric mercury, because of its neurotoxicity, long persistence and high bioaccumulation, is defined as a global pollutant that poses a threat to the health of the global population. Especially the organic form of mercury, like methylmercury (MeHg), is associated with neurocognitive deficits in human fetuses and cardiovascular effects in adults (Axelrad et al., 2007; Roman et al., 2011). In order to protect human health and the environment from adverse effects of mercury, a legally-binding international treaty Minamata Convention on Mercury was adopted in October 2013 and entered into force in August 2017 (UN Environment, 2017). The Minamata Convention requires parties to reduce mercury emissions and to assess the effectiveness of mitigation measures. China is one of the world's largest mercury emitters as well as the signatory to the Minamata Convention. The annual atmospheric mercury emissions in China were about 565 tons in 2015, accounting for about a quarter of global anthropogenic mercury emissions (AMAP/UNEP, 2018). The predominant anthropogenic Hg emission sources in China were industrial coal combustion, coal-fired power plants, nonferrous metal smelting, and cement production (Zhang et al., 2015). The characteristics of Hg emissions such as large emission amount and industrial production-dominated emissions made that China has great potential to reduce mercury emissions through the implementation of the Minamata Convention on Mercury. A mercury emissions inventory of China for 1978 – 2014 has reported that anthropogenic mercury emissions peaked in 2011 and then showed a downward trend (Wu et al., 2016). In addition, China had reduced anthropogenic mercury emissions by 127 tons from 2013 to 2017 (Liu K. et al., 2019). Among them, mercury emissions from the coal-fired power plants fell from 105 tons in 2007 to 73 tons in 2015 (Zhang et al., 2015; Liu et al., 2018). China has introduced a series of air cleaning measures including upgrading precipitator devices, newly built desulfurization and denitrification devices and ultra-low emission renovations since 2013, which led to synergistic removal of mercury (Liu K. et al., 2019). Strict restrictions of mercury on the mining, production, utilization, import and export have also been imposed in China since 2017 (https://www.mee.gov.cn/, last access: 17 May 2022).

Atmospheric mercury is usually classified into three categories according to the determination technique: gaseous elemental mercury (GEM), gaseous oxidized mercury (GOM) and particulate bound

28　mercury (PBM). Because of its stability and volatility, GEM is the dominant form of atmospheric

29　mercury, accounting for up to 95%. GEM has an atmospheric residence time of 0.5 – 2 years and can

30　spread globally before being deposited to earth's surfaces (Schroeder and Munthe, 1998; Zhang et al.,

31　2013; Yuan et al., 2021). On the other hand, GOM and PBM have relatively high reactivity and dry/wet

32　deposition rates and are therefore easier to be removed from the atmosphere. Field observations are vital

33　to understand the long-term variation of Hg levels in the atmosphere. There are some global and regional

34　mercury monitoring networks around the world which provided a long-term monitoring result. For

35　example, a steep decline trend of GEM concentrations (0.05 ng m^{-3} yr^{-1}) was observed at Mace Head,

36　Ireland, from 2013 to 2018 (Custodio et al., 2020), while GEM data from Cape Point, South Africa,

37　showed a slight increase from 2007 to 2017 (Slemr et al., 2020). China has also carried out a series of

38　observational studies in the past two decades. These observation studies on GEM concentrations mostly

39　focused on 1 – 2 years, and few continuous GEM observation records over multiple years in China were

40　published (Fu et al., 2015). A three-year measurement at Chongming Island, East China, showed that the

41　annual GEM concentrations significantly decreased from 2.68 ng m^{-3} in 2014 to 1.60 ng m^{-3} in 2016, at

42　a rate of -0.60 ± 0.08 ng m^{-3} yr^{-1} (Tang et al., 2018). Whereas, a multi-year observation of GEM in

43　Guiyang, Southwest China, showed an increasing trend from 8.40 ng m^{-3} in 2002 to 10.2 ng m^{-3} in 2010,

44　and the increase mainly occurred during the cold season (Fu et al., 2015).

45　　The variation of GEM concentrations is influenced by a variety of factors such as anthropogenic

46　emissions, meteorological conditions, as well as intra- and inter-regional transport (Tang et al., 2018; Liu

47　C. et al., 2019; Zhang et al., 2021). In previous studies, the impact of anthropogenic emissions changes

48　was often quantified by compiling emission inventories (Zhang et al., 2015; Wu et al., 2016; Liu K. et

49　al., 2019; Cai et al., 2020). The trajectory-based analysis method was frequently applied to analyze the

50　impact of regional transport (Tang et al., 2018; Wang et al., 2021). However, the results like the impacts

51　of anthropogenic emissions and regional transport derived from above different method systems could

52　not be comparable. Generalized additive models (GAMs), a regression analysis method, are data-driven

53　and able to incorporate non-linear relationships of air pollution with numerical and categorical variables,

54　which have been introduced into influencing factor identification in recent years (Wood and Augustin,

55　2002). The impact of local anthropogenic emissions, regional transport, and meteorological factors on

GEM concentrations in Nanjing, East China was quantified by using the GAMs (Zhang et al., 2021).

GAMs were also used to explain the decline of GEM concentrations in Beijing and the result showed

that reduction of anthropogenic mercury emissions, variation in meteorological conditions, and change

in globe background level explained 51.5%, 47.1% and 1.4% of the decrease in GEM concentrations,

respectively (Wu et al., 2020). It can be seen that GAMs are a promising tool to explore the effect of

factors like anthropogenic emissions and natural perturbations on GEM concentrations.

China has adopted aggressive atmospheric control measures in the last decade. Long-term GEM

observation was very necessary to investigate the variation of GEM levels and its influencing factors. In

this study, GEM, conventional pollutants and meteorological parameters were simultaneously observed

in Xiamen, a coastal city in Southeast China, in January (represents winter) and July (represents summer)

over the period 2012 – 2020. The main objectives of this study are: (1) to characterize the inter-annual,

seasonal and diurnal variations of GEM in Xiamen, a coastal city of Southeast China, (2) to identify the

source regions of GEM on a local and regional scale and their influence on annual concentrations of

GEM, (3) to investigate the influencing factors including anthropogenic emissions, regional transport

and meteorology on the inter-annual variation of GEM concentrations in the study region.

2 Method

2.1 Site description

The study site (Xiamen, 118°04'13''E, 24°36'52''N) is located in the Institute of Urban Environment,

Chinese Academy of Sciences in Jimei District of Xiamen City, Fujian Province, China (Fig. 1a). The

site was characterized by a typical subtropical monsoon climate, with the prevailing ocean monsoon in

summer and northerly or northeasterly air masses from the inland of China in winter. Industrial point

sources were mainly distributed to the northeast and the southwest of the study site (Fig. 1b). The

instruments were placed on the roof of a building (~80 m above the ground). The outdoor air inlet of the

sampling unit was located at 2 m above the rooftop of the building.

5
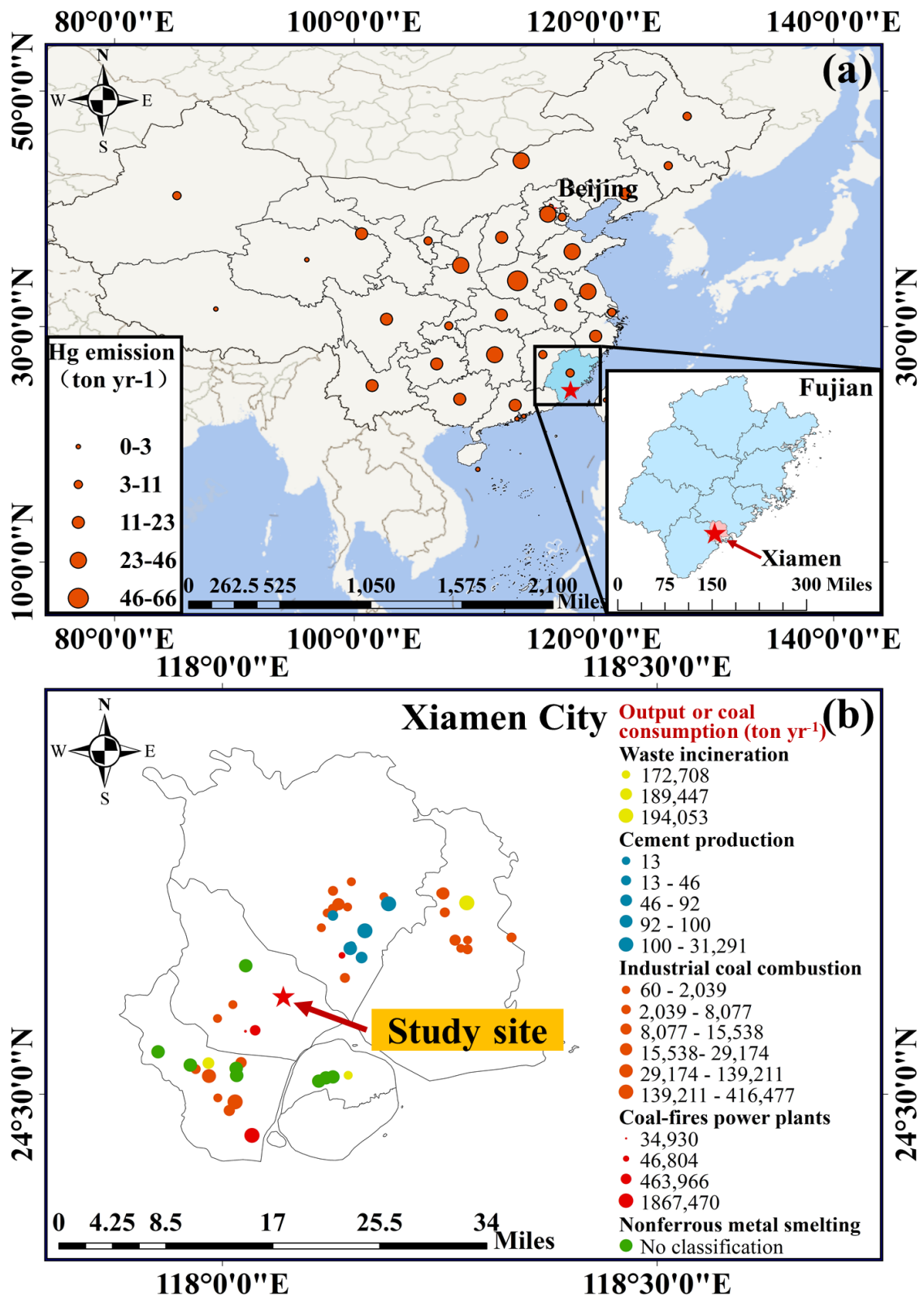
Figure 1. (a) The location of study site in Xiamen City, Fujian Province, China and the regional distribution map of anthropogenic Hg emissions in China in 2014 (Wu et al., 2016). Note that the red dots represent the amount of mercury emitted by each province. (b) The distribution of local industrial point sources in Xiamen. Note that the colors of the dots represent different industrial categories, and the size represents a company's output or coal consumption (ton yr^{-1}).

2.2 Atmospheric mercury measurements

86

87   **Instrument operation:** Atmospheric mercury was measured by the Tekran 2537B/1130/1135 system
88   (Tekran Inc., Toronto, Canada). During the 1 h sampling period, the GOM and PBM were first collected
89   onto the KCl-coated quartz annular denuder and the quartz filter respectively, and GEM concentrations
90   were measured by a Tekran 2537B Hg vapor analyzer every 5 min at a sampling flow rate of 1 L min^{-1}.
91   The detection limit of GEM measurement was 0.06 ng m^{-3}. In the following 1 h desorbing phase, the
92   PBM and GOM were sequentially desorbed and then quantified by the Tekran 2537B. The principle and
93   the routine maintenance of the equipment in detail have been described in the previous study (Xu et al.,
94   2015). The Tekran 2537B analyzer was calibrated automatically every 25h using the internal Hg
95   permeation source inside the instrument, and the accuracy of this permeation source was calibrated every
96   12 months with manual injection of Hg by a syringe from an external Hg source (Module 2505).

97   **Hg species selection**: GEM has a low chemical reactivity comparing to GOM and PBM in the
98   atmosphere. GEM concentrations are largely affected by factors like anthropogenic emissions and
99   atmospheric physical processes, which could be well represented by conventional pollutants like CO and
100   meteorological parameters like BLH. Whereas, GOM and PBM concentrations were strongly affected
101   by chemical transformation processes, which has no known suitable indicators. In addition, involving
102   chemical transformation effect as a main factor in the GAM models would make it more complicate.
103   Thus, we used the statistic method to explore the influencing factors on the more stable Hg species, GEM
104   in this study.

105   **Observation period selection:** This study was based on the GEM observation data of January and
106   July (representative of winter and summer, respectively) in 2012, 2013, 2015, 2017 and 2020. There was
107   a different time period of instrument malfunction among years. To ensure the study time periods were
108   consistent and the data could be comparable among years, we chosen the representative months of GEM
109   data in this study. Xiamen is located in the coastal region of Southeast China under the control of
110   subtropical oceanic monsoon, which has a significant distinction in meteorology between summer and
111   winter. According to the climate features in the study region, January and July well reflect the
112   characteristic of the winter and summer seasons, respectively. In addition, a whole year GEM
113   concentration observation in Xiamen supported that the GEM data in January can represent the GEM

114   characteristics of winter and July can represent summer (Xu et al., 2015). In order to match other

115   parameters, the time resolution of GEM concentrations was converted from the original 5 min to 2 h. For

116   most of the data (70%) during the study period, the proportion of GOM and PBM in TGM was less than

117   5%. Thus, GEM concentrations in this study were directly compared to TGM in the below analysis.

118   **2.3 Meteorological parameters and criteria air pollutants**

119   In this study, the conventional pollutants (including SO_2, NO_2, O_3, CO, PM_{10}, $PM_{2.5}$) and

120   meteorological parameters (including wind speed (WS), wind direction (WD), relative humidity (RH),

121   air temperature (T) and surface air pressure (SP)) were obtained from Xiamen air quality monitoring

122   station. Note that above pollutants concentrations and meteorological data were averaged into 2 h time

123   intervals. Other meteorological parameters: boundary layer height (BLH), downward UV radiation at the

124   surface (UVB) and low cloud cover (LCC) were obtained from the European Centre for Medium-Range

125   Weather Forecasts (ECMWF) reanalysis (https://www.ecmwf.int, last access: last access: 23 March

126   2022).

127   **2.4 Concentration weighted trajectory (CWT)**

128   Hybrid Single-Particle Lagrangian Integrated Trajectory (HYSPLIT) model and Global Data

129   Assimilation System data (https://www.arl.noaa.gov/, last access:5 May 2022) were applied to calculate

130   the 72h backward air mass trajectories. The interval of backward trajectories was 2 h and the arrival

131   height was set as 500 m above the ground level.

132   Concentrations-weighted trajectories (CWTs) analysis is useful to identify pollution sources spatially

133   for long-term environment measurement (Cheng et al., 2013). The principal of the CWT method is that

134   each grid cell is assigned a weighted concentration by averaging the sample concentrations associated to

135   trajectories that cross that grid cell as follows:

$$C_{ij} = \frac{1}{\sum_{l=1}^{M} \tau_{ijl}} \sum_{l=1}^{M} C_l \, \tau_{ijl} \tag{1}$$

136   Where C_{ij} is the average weighted concentration in the ijth cell, l is the index of the trajectory, M is

137   the total number of trajectories, C_l is GEM concentration observed on arrival of trajectory l, τ_{ijl} is the

138   time spent in the ijth cell by trajectory.

139   Based on the maximum distance travelled by the 72h back trajectories over the study period, a

140   geographical domain from 17° to 60 N and from 45° to 135° E (from 4° to 37° N and from 100° to 153°

141   E) was found to be suitable in January (July). This domain encompassed the locations of nearly all the

142   trajectory segment endpoints from all the back trajectories. The resolution for CWT was $1° \times 1°$ in this

143   study.

144   **2.5 Model development**

145   Generalized Additive Models, a regression analysis method, have been used to establish the

146   relationship between GEM and various variables, and to investigate the influencing factors on the inter-

147   annual trend of GEM concentrations (Gong et al., 2017). The models were run by the following steps:

148   parameter selection, model establishment, and model quality control.

149   **Parameter Selection:** 16 variables we obtained from site observation and web downloads generally

150   fell in four categories: anthropogenic emissions (SO_2, NO_2, O_3, CO, $PM_{2.5}$, PM_{10}), surface meteorology

151   (T, RH, WS, WD, SP), high-altitude meteorology (BLH, UVB and LCC) and air transportation (24h-

152   Latitude and 24h-Longitude) (Table S1). All the variables were standardized by min-maximum method.

153   The normalized data eliminates the effects of differences in dimension and ranges of values between

154   indicators. The standardized variables were then screened using two methods: Statistical judgment and

155   the meaning of the variables. Firstly, the collinearity diagnosis method was adopted to make judgment

156   according to the variance inflation factor (VIF). $PM_{10,}$ SO_2, NO_2, SP and UVB were rejected into the

157   model due to their high collinearity (VIF > 5). Secondly, we considered the meaning of the remaining

158   parameters. Parameters O_3 and $PM_{2.5}$ were easily rejected into the model. CO is mainly sourced from

159   anthropogenic emissions and has a long atmospheric residence time (compared to SO_2 and NO_2). In

160   addition, Hg emissions in Fujian provinces were dominated by combustion sources (Liu K. et al., 2019).

161   Hence, we used CO to represent anthropogenic Hg emissions. After determining the first parameter CO,

162   we put the remaining parameters (WS, WD, T, RH, BLH, LCC, 24h-Latitude and 24h-Longitude) into

163   the model one by one. The performance of GAMs was judged according to Akaike Information Criterion

164   (AIC) and R^2 values. Specifically, as the parameters were successively added into the model, the AIC

165   decreased and R^2 increased. In this step, WS, WD and LCC were rejected. Based on this method, 6

9

166 variables including CO, RH, T, BLH, 24h-Latitude and 24h-Longitude were eventually selected into the

167 model (Table S2).

168 Considering that parameters of the same category might interact, we used interaction functions of

169 tensors. RH, T and BLH interaction was used to represent the meteorological factor. 24h-Latitude and

170 24h-Longitude interaction, which indicates the backward trajectory endpoint location during last 24 h

171 was used to represent the transportation factor. Given that the 6 selected variables passed the collinearity

172 test, the three factors anthropogenic Hg emissions represented by CO, meteorological factor represented

173 by RH, T, and BLH interaction, and transportation represented by 24h-Latitude and 24h-Longitude

174 interaction were considered to be independent of each other. Those selected variables were used in the

175 following model establishment.

176 **Model establishment:** GAMs were performed using R version 4.1.2 with the "mgcv" package. The

177 equation can be described as follows:

$$g(\mu) = f_1(x_1) + f_2(x_2) + \cdots + f_k(x_k) + \varepsilon, \tag{3}$$

178 Where x_j (j = 1, 2, 3, …, k) are different meteorological predictors and f_j is a smooth function of the

179 predictors; ε is the residual; μ is the expected value of the response variable; and g is the link function

180 specifies the relationship between the non-linear formulation and the expected value. We used the

181 "identity link" function with a Gaussian distribution because the relationship between GEM and the three

182 factors conformed to a Gaussian distribution and the estimation of GAMs was considered unbiased. In

183 order to ensure the balance between under-fitting and overfitting of observation data, we used a penalized

184 cubic regression as a smooth function. In the running process of the model, the concentration contribution

185 of the smoothed independent variable (anthropogenic emissions, meteorological effects, and

186 transportation) to the dependent variable (GEM) was output and converted into contribution ratio, which

187 is helpful to determine the degree of each variable driving the prediction. To eliminate the effect of

188 seasonality on variance clustering, we used "seasons" as an input variable when building the model with

189 the whole dataset, and then run the model separately in summer and winter.

190 **Model Quality Control:** The accuracy of GAMs simulation was assessed using a 10-fold cross-

191 validation test. The principle of the test is dividing the whole dataset into ten subsets randomly, and in

192 each round of cross-validation, nine subsets are used to fit the model and the remaining one is predicted.

10

193   This process was repeated 10 times to ensure that every subset was tested. The 10-fold cross-validation

194   results showed a good coincidence between the GAMs and cross-validated results ($R^2 = 0.89$, Fig. S1),

195   demonstrating the reliability of the established model. In order to test the underlying assumptions of

196   homogeneity, normality and independence of GAMs to ensure the validity and accuracy of the model,

197   we used the following methods (Fig. S2): (1) Quantile-quantile (QQ) plots (Sample quantiles against

198   theoretical quantiles), (2) scatterplots (residuals against linear predictor), (3) histograms of the residuals

199   and (4) scatter plots (response against fitted value). The QQ-plot showed that the GAMs produced good

200   results around the average concentrations and the residuals showed a normal distribution.

201   **3 Results and discussion**

202   **3.1 Temporal variations of GEM concentrations**

203   **3.1.1 Inter-annual variation**

204   Monthly concentrations of GEM ranged from 3.50 to 4.47 ng m^{-3} in January and 1.56 to 2.65 ng m^{-3}

205   in July during the whole study period, with mean values of 4.04 ± 1.01 ng m^{-3} and 2.29 ± 0.83 ng m^{-3},

206   respectively. The GEM concentrations in Xiamen were several times higher than the Hemisphere

207   background concentrations (~1.5 ng m^{-3}) (Sprovieri et al., 2016; Diéguez et al., 2019). Comparisons of

208   TGM/GEM concentrations in Xiamen with other urban and rural areas in East Asia over the last decade

209   are shown in Table 1. The mean concentrations of GEM mostly fell in a range of 2 – 5 ng m^{-3} in East

210   Asia (except for some background sites). The winter GEM concentrations in Xiamen was slightly higher

211   than those measured at rural and background monitoring sites such as Changdao Island, Tibetan Plateau

212   region, and Mt. Ailaoshan (Zhang et al., 2016a; Yin et al., 2018; Wang et al., 2020), while lower than

213   those reported from inland urban sites like Lanzhou, Nanjing, and Shanghai (Zhu et al., 2012; Duan et

214   al., 2017; Yin et al., 2020). The summer GEM concentrations in Xiamen were relatively low, comparable

215   to those of Changdao Island, Yongheung Island and Fukuoka (Marumoto et al., 2015; Lee et al., 2016;

216   Wang et al., 2020).
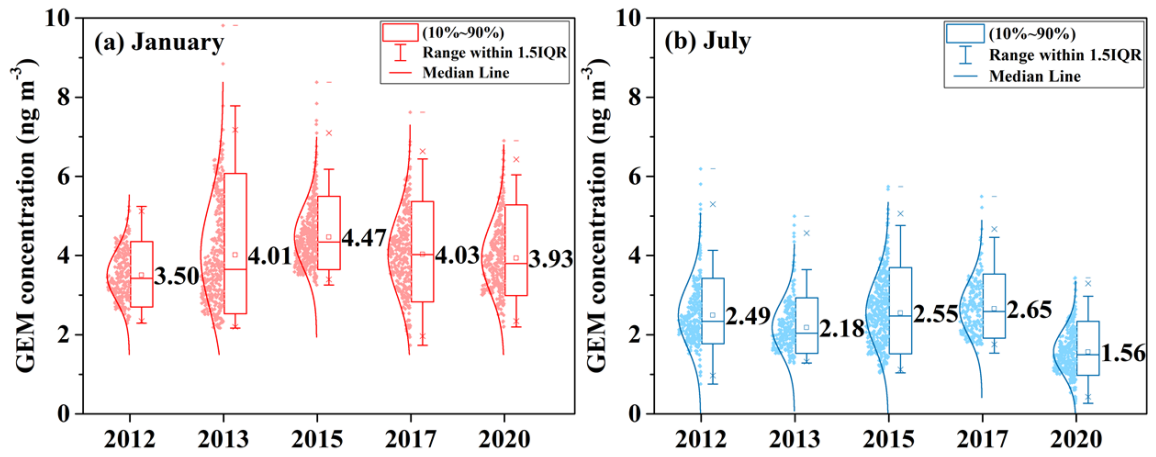
Figure 2. Statistical summaries of gaseous elemental mercury (GEM) concentrations in Xiamen in (a) January and (b) July of the study years.

Table 1. Comparisons of TGM/GEM concentrations in Xiamen with other urban and rural areas in East Asia over the period 2010 – 2020.

Locations	Classification	Time	TGM/GEM (ng m^{-3})	Winter	Summer	References
Xiamen, CN	Suburban (Coast)	03/2012–02/2013	3.50±1.21	/	/	(Xu et al., 2015)
Mt. Changbai, CN	Rural	07/2013–07/2014	1.68±0.47	/	/	(Liu C. et al., 2019)
Haidian, CN	Urban	02/2018–03/2018	2.77±0.91	/	/	(Wang et al., 2021)
Shanghai, CN	Suburban	06/2014–12/2014	4.19±9.13	5.5±6.6	3.8–5.3	(Duan et al., 2017)
Shanghai, CN	Suburban	12/2015–02/2016	2.77±1.36	2.88	2.87	(Qin et al., 2019)
Hefei, CN	Suburban	07/2013–06/2014	4.07±1.91	4.05 ± 1.81	4.08±1.99	(Hong Q. et al., 2016)
Ningbo, CN	Coastal	04/2011–04/2013	3.30±1.40	3.70	2.60	(Yu et al., 2015)
Ningbo, CN	Urban (Coastal)	07/2013–01/2014	3.26±1.63	/	/	(Hong Y. et al., 2016)
Ningbo, CN	Urban (Coastal)	12/2016–11/2017	2.44±0.95	2.62±1.05	2.26±0.78	(Yi et al., 2020)
Nanjing, CN	Urban	01/2011–12/2011	7.94±6.99	5.5±2.5	9.9±8.2	(Zhu et al., 2012)
Mt. Ailaoshan, CN	Rural	05/2011–05/2012	2.09±0.63	2.04±0.58	2.20±0.60	(Zhang H. et al., 2016)
Taoyuan city, Taiwan, CN	Suburban	10/2017–09/2018	2.61±6.47	2.19±0.75	2.27±1.67	(Sheu et al., 2019)
Taichung city, Taiwan, CN	Rural	10/2014–09/2015	1.19	/	/	(Fang et al., 2017)
Yongheung, Korea	Island	01/2013–08/2014	2.80±1.10	3.50–3.70	2.30±0.90	(Lee et al., 2016)
Gyodong Island, Korea	Rural	08/2015–09/2017	2.70±2.60	2.8±2.9	1.70±1.0	(Lee et al., 2019)
Fukuoka, Japan	Urban	06/2012–05/2013	2.33±0.49	2.31±0.44	2.37±0.58	(Marumoto et al., 2015)
Nam Co, Tibetan Plateau, CN	Plateau	01/2012–10/2014	1.33±0.24	1.14±0.18	1.50±0.20	(Yin et al., 2018)
Changdao Island, CN	Rural (Coastal)	10/2013–07/2015	2.52±0.82	2.87±1.16	2.25±0.51	(Wang et al., 2020)
Lanzhou, CN	Urban	10/2016–10/2017	4.48±2.32	5.06±2.45	4.45±2.10	(Yin et al., 2020)

221   The inter-annual variability of GEM concentrations in January and July are shown in Fig. 2. The GEM

222   concentrations in Xiamen showed a minor variation between years. Specifically, GEM concentrations in

223   January were lowest in 2012 (3.50 ng m^{-3}), highest in 2015 (4.47 ng m^{-3}), and comparable in the years of

224   2013, 2017 and 2020. Whereas GEM concentrations in July was highest in 2017 (2.65 ng m^{-3}) and

225   significant lowest in 2020 (1.56 ng m^{-3}). According to the published data, Wu et al. (2016) estimated

226   atmospheric Hg emissions in China decreasing from 547 tons in 2010 to 530 tons in 2014. The report

227   from AMAP/UNEP showed that the anthropogenic Hg emissions in China were 565.2 t in 2015 relative

228   to 575.2 t in 2010 (AMAP/UNEP, 2018). An inventory over the period 1978-2017 revealed that China's

229   anthropogenic Hg emission was highest in 2013 and then decreased until 2017 (Liu K. et al., 2019). It

230   could be expected that the anthropogenic Hg emissions in China had a downward trend over the period

231   2012-2020 and the peak emission was most likely to occur in 2012 to 2014 (Fig. S3,4). Recent studies

232   have indicated either a stable or a slight decreasing trend for GEM or TGM concentrations in Chinese

233   cities after 2013 when China has applied the vigorous measures to control air pollution (Qin et al., 2020;

234   Wu et al., 2020; Yin et al., 2020). For instance, it was reported that GEM concentrations at Chongming

235   Island in East China significantly decreased from 2014 to 2016, and the inflection point occurred before

236   2014 (Tang et al., 2018). Note, those measurements mostly lasted for 2 – 4 years. So far, the observations

237   of GEM concentrations over a long time period were scarce. Our result suggests the influencing factors

238   on the variation of GEM in East China would be complex over the last decade.

239   Coal combustion is one of the leading mercury sources in China (Wu et al., 2006). Table S3 summaries

240   the consumption of coal and the statistics of annual SO_2 and NOx emissions in Fujian Province over the

241   period 2012 – 2020. The coal consumption in Fujian and China exhibited a similar variation, firstly

242   decreasing to a valley in 2016 and then showing an upward trend from 2016 to 2020 (Fig. S5). Whereas,

243   there was a decreasing trend for SO_2 and NOx emissions during the whole study period, with a most

244   remarkable reduction of emissions in 2016. In 2013, the Chinese State council issued an air pollution

245   prevention and control action plan. Since then, plenty of emissions control measures, like accelerate the

246   elimination of backward production capacity, accelerate the promotion of central heating, upgrade and

247   building air pollution control devices, have been widely implemented in China. Previous studies have

248   found that mercury can be synergistically removed in the process of desulfurization and de-nitration

14

249 (Zhang Y. et al., 2016; Liu K. et al., 2019). The installation of selective catalytic reduction to control

250 nitrogen oxide emissions is often accompanied by the oxidation of GEM to GOM, and the combined

251 application of selective catalytic reduction and flue gas desulfurization could further reduce TGM

252 emissions to the atmosphere (Rallo et al., 2012). Nonetheless, the inconsistent inter-annual variation in

253 GEM concentrations and SO_2/NOx emissions indicates that additional factors, like GEM emission

254 sources other than coal combustion and/or meteorological changes strongly affected the inter-annual

255 variation trend of GEM in the study region.

256 **3.1.2 Seasonal and diurnal patterns**

257   The GEM concentrations in Xiamen were approximately 1.41 – 2.52 times higher in winter than in

258 summer ($P < 0.001$, one-way ANOVA) over the study years. The similar seasonal variation was widely

259 observed in cities including Shanghai, Ningbo, Lanzhou, and Yongheung, as well as Gyodong Island,

260 and Changdao Island (Yu et al., 2015; Hong Y. et al., 2016; Lee et al., 2016; Duan et al., 2017; Lee et

261 al., 2019; Wang et al., 2020; Yi et al., 2020; Yin et al., 2020). However, a reverse seasonal variation with

262 higher GEM in summer than in winter was observed in Nanjing, Chongming Island, Mt. Ailaoshan and

263 Tibetan Plateau region (Zhu et al., 2012; Zhang H. et al., 2016; Tang et al., 2018; Yin et al., 2018). There

264 were many factors responsible for the seasonal variation of GEM in Xiamen. In terms of Hg emission

265 sources, local industrial emissions were relatively stable over the course of a year. The key factor with

266 seasonal changes was the increased usage of coal for heating which mainly occurred in northern China

267 in cold seasons. Although there was no coal consumption for heating in southern China, GEM is well

268 mixed due to its prolonged lifetime (0.5–2 years) (Schroeder and Munthe, 1998; Zhang et al., 2013).

269 Monsoons change the source–receptor relationships at observation sites, and thus affect the seasonal

270 variation of GEM concentrations (Fu et al., 2015; Liu C. et al., 2019). For Xiamen, air masses in winter

271 mainly originated from north directions which passed through numerous intensive anthropogenic GEM

272 emissions areas (Fig. 1a), while air mass in summer mainly originated from ocean with less GEM point

273 sources. Another important factor is that the mixing heights were reduced due to stable inversion layer

274 in winter. As a result, GEM diffused slowly and accumulated easily in the surface layer. In addition, for

275 the sites in the Northern Hemisphere, the greater removal of GEM by wet and dry deposition could also

276 lead to lower GEM concentrations in warmer seasons (Fu et al., 2008; Tang et al., 2018).

277   The diurnal variations of bihourly GEM concentrations were consistent among years (Fig. 3). In

278   general, the GEM concentration peaked in the early morning, decreased to a valley in the afternoon, and

279   then rose during the night. The diurnal pattern of GEM concentrations in January 2015 were gentle than

280   other years of the same period, which might be related to the enhanced effect of air mass transport (Fu et

281   al., 2012; Nguyen et al., 2022). The diurnal pattern of GEM concentrations in Xiamen is consistent with

282   other urban sites like Guiyang, Hefei and Guangzhou (Feng et al., 2004; Chen et al., 2013; Fu et al.,

283   2015). Previous studies often attributed diurnal variations of GEM to the effect of various anthropogenic

284   emissions, photochemical oxidation and the diurnal variation of BLH (Hong Y. et al., 2016; Duan et al.,

285   2017). The diurnal pattern of GEM in Xiamen was similar to those of SO_2, NO_2 and CO (Fig. S6a – c),

286   reflecting the combined effects of common anthropogenic emissions and the diel fluctuation in

287   meteorology. The decreasing trend of GEM from early morning to afternoon was likely related to the

288   intensified turbulent mixing in the boundary after sunrise while the nighttime had the opposite condition

289   (Fig. S6d). The photo-oxidation of GEM might contribute a small part to the diurnal variation of GEM,

290   but it was not the dominant factor for the daytime GEM reduction due to its low reaction rate in the study

291   region.
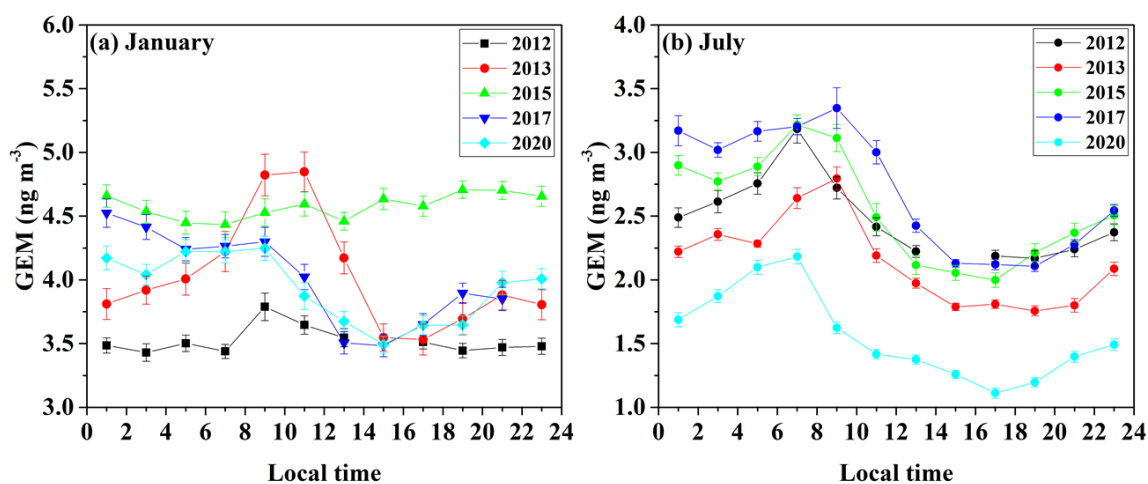
292

293   **Figure 3. The diurnal trend of GEM concentrations in (a) January and (b) July over the study years. Note**

294   **that the value of error bars has been reduced tenfold.**

3.2 Potential source regions of GEM

3.2.1 Local emissions

According to the industrial Hg emissions inventory in China, the main Hg emissions industries included industrial coal combustion, coal-fired power plants, non-ferrous metal smelting, cement production, and waste incineration (Zhang et al., 2015; Wu et al., 2016). The relationships between the spatial distribution of industrial sources and bivariate polar plots of GEM concentrations would shed light on the influence of local anthropogenic point sources (within Xiamen city) on GEM concentrations. As shown in Fig.4a, 4d, the elevated GEM concentrations in the bivariate polar plots of individual seasons were highly concentrated, suggesting that the spatial distribution of main Hg point sources was similar among years. However, the polar plot results of GEM concentrations were distinctly different between seasons likely due to the shift in the dominant wind. In January, the elevated GEM concentrations were associated with west wind with a low WS of $0.5 - 2.0$ m s^{-1} (Fig. 4a), which indicates nearby emission sources. They were likely the industrial coal combustion, and non-ferrous metal smelting upwind from the west of the monitoring site (Fig. 1b). The conventional pollutants are the good indicators of primarily anthropogenic sources. In Xiamen city, the coal-fired power plants contributed 57.8% of local industrial SO$_2$ emissions and 62.4% of CO industrial emissions (Air pollution emissions inventory of Xiamen city in 2016, unpublished report). A close correlation of GEM with SO$_2$ and CO in westerly WD with low speeds (Fig. 4b, 4c) further supported above conclusion that the contributions of local industrial sources to GEM.

In July, the elevated GEM concentrations occurred when winds came from the southwest with the WS about $2.5 - 3$ m s^{-1} (Fig. 4d). As shown in Fig. 1b, there are many industrial clusters in the southwest direction of the observation site including coal-fired power plants, industrial coal combustion and nonferrous metal smelting. Accordingly, we suspected that the local industrial clusters upwind of the southwest to the study site caused an evident increase in GEM concentrations. High WS of the southwest wind likely weakened the correlation between GEM and SO$_2$ (Fig. 4e) while GEM and CO remained a good correlation in the southwest wind due to their stable chemical properties (Fig. 4f). Another elevated GEM concentration condition occurred when wind came from the east with a lower WS of $0 - 2$ m s^{-1} (Fig. 4d). Such low WS suggests a stagnant meteorological condition which was unfavorable for GEM

323   dispersion. In addition, GEM and SO$_2$ showed a good correlation in the case of the east wind with WS

324   of 1 – 2 m s^{-1}. Hence, we could speculate that the upwind point sources, like industrial coal combustion

325   and nonferrous metal smelting, as well as the adverse atmospheric diffusion conditions contributed to the

326   increasing GEM concentrations. As shown in Table S4, GEM in Xiamen was overall positively correlated

327   with SO$_2$, NO$_2$, CO and PM$_{2.5}$, but the correlation coefficient fluctuated remarkably among years. In

328   addition, the inter-annual variation of GEM concentrations was not coincided with those of SO$_2$ or NO$_x$

329   emissions as mentioned above. Thus, the contribution of local Hg point sources to atmospheric GEM

330   varied among year and it could not fully explain the inter-annual variation of GEM concentrations in the

331   study region.
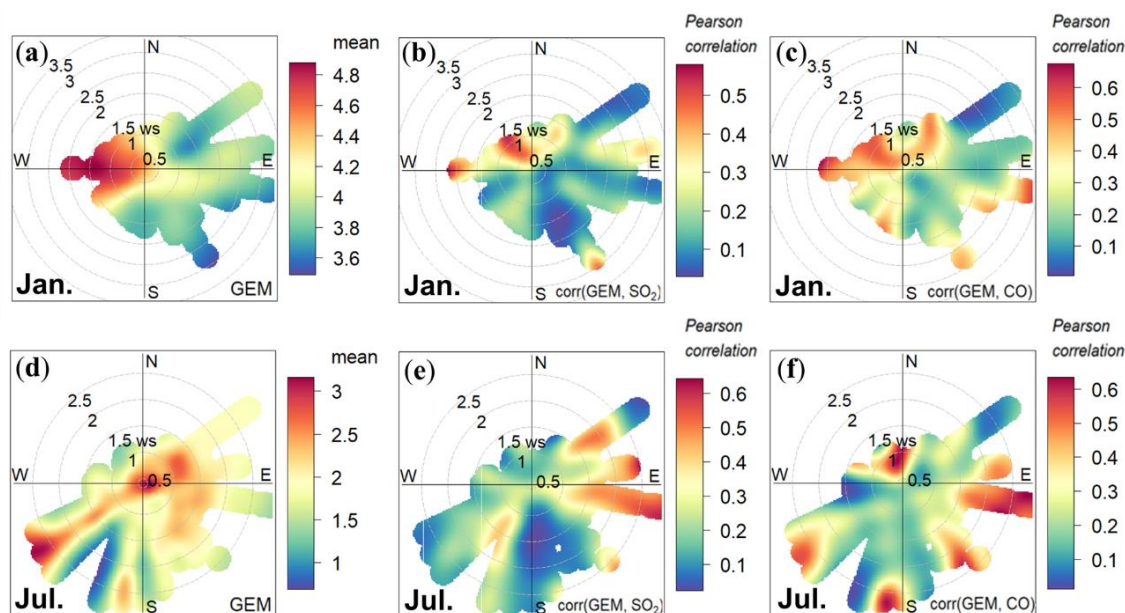
332

333   **Figure 4. Bivariate polar plots of GEM concentrations (a, d), the correlation coefficients of GEM with SO₂ (b,**

334   **e) and CO (c, f) as a function of WS and WD in January and July during the whole study period. Note that**

335   **GEM in ng m⁻³, wind speed in m s⁻¹, wind direction in °.**

336   **3.2.2 Long distance migration**

337   The result of CWT analysis based on HYSPLIT backward air mass trajectories are shown in Fig. 5.

338   On the whole, the GEM concentrations in Xiamen were under an influence of continental air masses in

339   January and a mixing influence of continental and marine air masses in July. To describe it better, the

340   potential source regions of GEM were marked as Fujian province, East China (EC), Southwest China

341   (SWC), North China (NC), Central China (CC), South China Sea (SCS), Philippines Sea and Taiwan

342　　Strait (PhiS+TW), as well as Philippines Sea and East China Sea (PhiS+ECS) (The details of region

343　　definition are presented in Supporting Information).

344　　　It can be seen that the higher weights of CWT mostly dominated in Fujian province and EC in January.

345　　The results could reasonably be expected because anthropogenic Hg emissions in East China was

346　　extremely large due to the dense industries (Zhang et al., 2015). The potential source regions for GEM

347　　in Xiamen also included ECS in January 2012, CC in January 2017, and PhiS+TW in January 2020. The

348　　North China Plain region was one of the heaviest mercury polluted area in China (Zhang et al., 2015),

349　　but to our surprise, it did not become an important source region for Xiamen GEM. This is most likely

350　　due to the effect of transmission distances, while GEM concentrations decreased with long transport

351　　distances. In contrast, short air mass trajectories, like from the Fujian province, indicated a relatively

352　　stagnant air condition which is not conducive to the diffusion of GEM (Zhang et al., 2021). The weights

353　　of CWT in January 2015 were higher than those of other study years and the region of high CWT values

354　　spread over Fujian province and EC. Previous studies have also reported the high levels of GEM in 2015

355　　among urban Beijing, Changdao Island, rural Shanghai and Chongming Island (Tang et al., 2018; Qin et

356　　al., 2020; Wang et al., 2020; Wu et al., 2020), which suggests a heavy GEM pollution on a large regional

357　　scale during 2015. The high GEM concentrations in January 2015 was likely due to a combination of

358　　high-level Hg emissions and adverse meteorological conditions. The annual atmospheric mercury

359　　emissions in China were about 565 tons in 2015, which was roughly 20% higher than those in 2010

360　　(AMAP/UNEP, 2018). According to anthropogenic mercury emissions inventory in China during 1978

361　　– 2017, mercury emissions might peak around 2013, and remained high in 2015 (Figure S2). In addition,

362　　an adverse effect of meteorological conditions due to extreme 2015 – 2016 El Niño event might also

363　　result in an increase of GEM concentrations in 2015 (Nguyen et al., 2022).

364　　　The dominant clean marine air masses helped explain the lower concentration of GEM in July than in

365　　January. As shown in Fig. 5, the dominant source region for GEM in Xiamen in July mostly were SCS

366　　and PhiS+TW. The evasion of GEM from the ocean to the atmosphere was reported to be an important

367　　natural source (accounting for 50%) (Mason, 2008). When under the control of marine air masses, the

368　　ocean emissions would become a significant source for GEM in the study region. The CWT values were

369　　extremely high in SCS in July 2012 and in PhiS+TW in July 2017, while the CWT values were elevated

370   in SCS and ECS in July 2015. The relatively high GEM concentrations for Xiamen in July 2017 was

371   likely associated with the contribution of extremely high GEM from PhiS+TW. The elevated GEM

372   concentrations for Xiamen in July 2015 passed more closely through Southeast Asia where the intense

373   biomass burning often occurred (Friedli et al., 2009; Sheu et al., 2013; Liu et al., 2016). A previous study

374   on Hainan Island also pointed to the possibility of long-range transport of GEM from Southeast Asia to

375   South China (Liu et al., 2016).
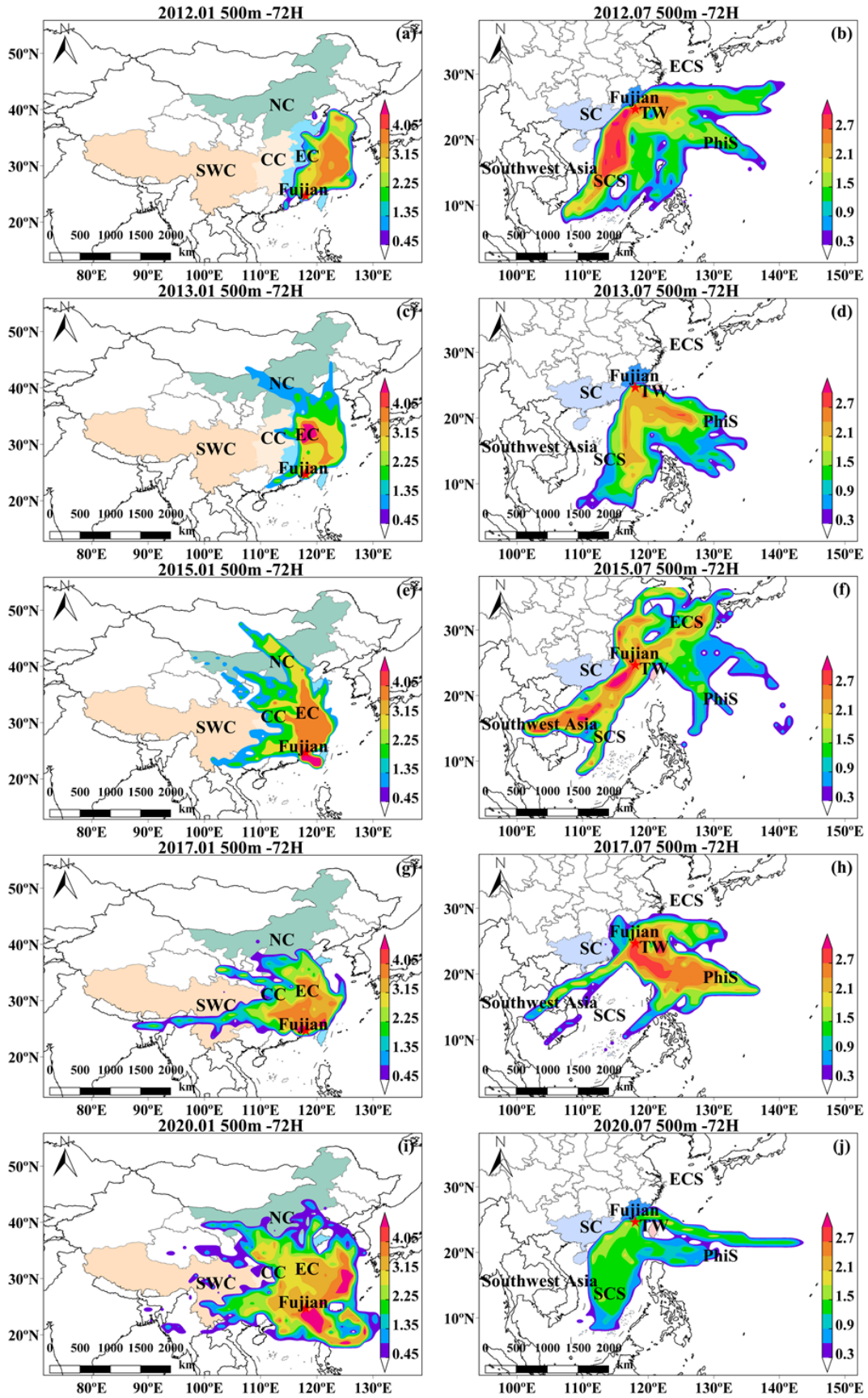
Figure 5. Concentration weighted trajectory (CWT) in January (a, c, e, g, i) and July (b, d, f, h, j) during the study years. The legend represents the weighted GEM concentrations (ng m^{-3}).

379 **3.3 Factors affecting GEM concentrations**

380 **3.3.1 Model evaluation**

381   GAMs were applied to investigate the influencing factors on the inter-annual variation of GEM in this

382 study. The fitted (observed) GEM concentrations derived from the GAMs were approximately $3.98 \pm$

383 0.47 ng m^{-3} (4.00 ± 0.84 ng m^{-3}) in January and 2.25 ± 0.41 ng m^{-3} (2.23 ± 0.61 ng m^{-3}) in July, reflecting

384 that the model approximates the concentration of GEM to the mean. The observed and fitted GEM

385 concentrations showed a good consistency in time series (Fig. 6a) and the residuals were normally

386 distributed (Fig. 6b). The R^2 of the observed and fitted GEM concentrations was 0.75 (Fig. S7) and the

387 variance interpretation rate was 75.8%. In previous studies using GAMs to quantify impact factors on air

388 pollutants, the R^2 was generally between 0.35 and 0.86 (Gong et al., 2018; Li et al., 2019; Wu et al., 2020;

389 Wu et al., 2021; Zhang et al., 2021). The fitted result of the GAMs in our study falls in this range.
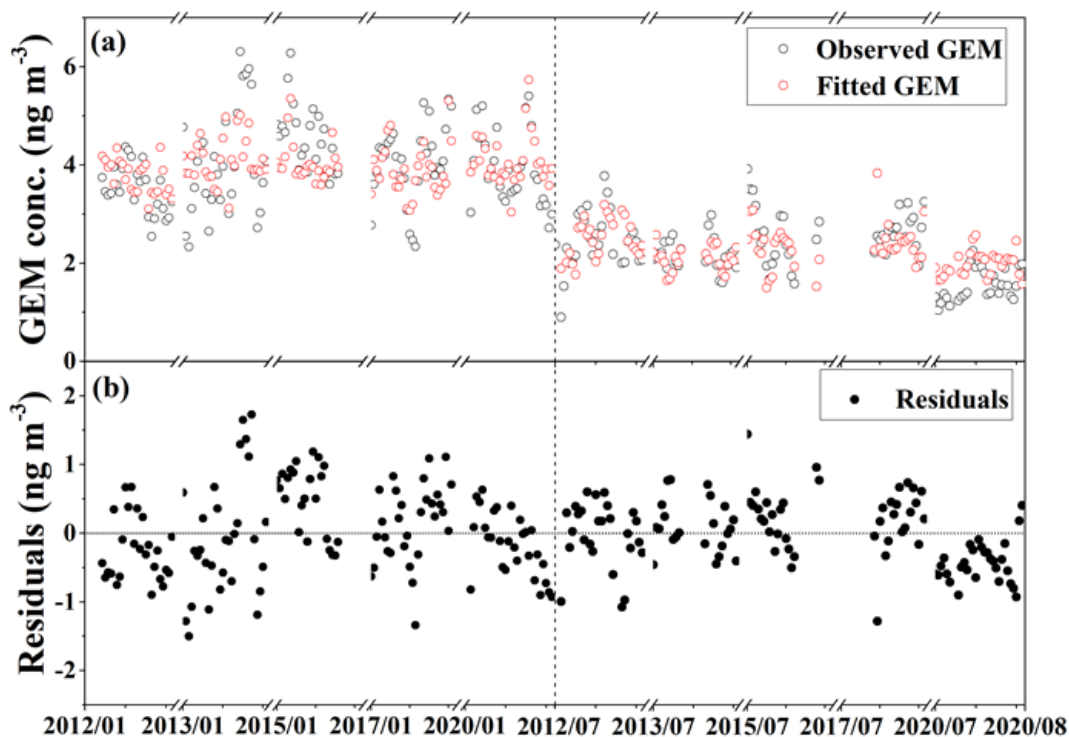
390

391 **Figure 6. Time series of (a) observed and fitted GEM concentrations in January and July and (b) residual**

392 **distribution during the whole study period.**

3.3.2 Inter-annual variations of factor contributions

The 6 screened variables represented the factors of anthropogenic emissions (CO), meteorology (T, RH, and BLH interaction) and transportation (24h-Latitude and 24h-Longitude interaction). The contributions of the three factors to the variation of GEM concentrations in January and July of the study years are shown in Fig. 7. The inter-annual interpretation rate of anthropogenic emissions varied from 27.8% to 50.8% in January and from 26.9% to 59.5% in July, with a mean value of 37.8 ± 11.9% during the whole study period. The interpretation rate of the emission factor to the variation of GEM concentrations was pronouncedly high in 2012 and decreased overall to 2020.China has adopted a series of desulphurization and denitrification measures for air pollution control during the period 2010 – 2015. The capacity of desulphurization and denitrification units in China had reached 99% and 92% of the total installed capacity of coal power plants, and 1.6×10^8 kw had been upgraded to achieve ultra-low emissions by 2015. In addition, strict restrictions of mercury on the mining, production, use, import and export were also be imposed in China since 2017 (http://www.mee.gov.cn, last access: 17 May 2022). We observed a positive relationship between GEM and the representative variable CO in most of the CO observed range (Fig. 8a, b). That is, GEM concentrations basically decreased with the reduction of CO which stands for anthropogenic emissions. The most significant reduction in GEM concentrations explained by anthropogenic emissions was 0.55 ng m^{-3} from July 2012 to July 2013 and 0.74 ng m^{-3} from January 2013 to January 2015. The results reveal that the vigorous air pollution control measures in China were very effective reducing GEM concentrations in the study region.
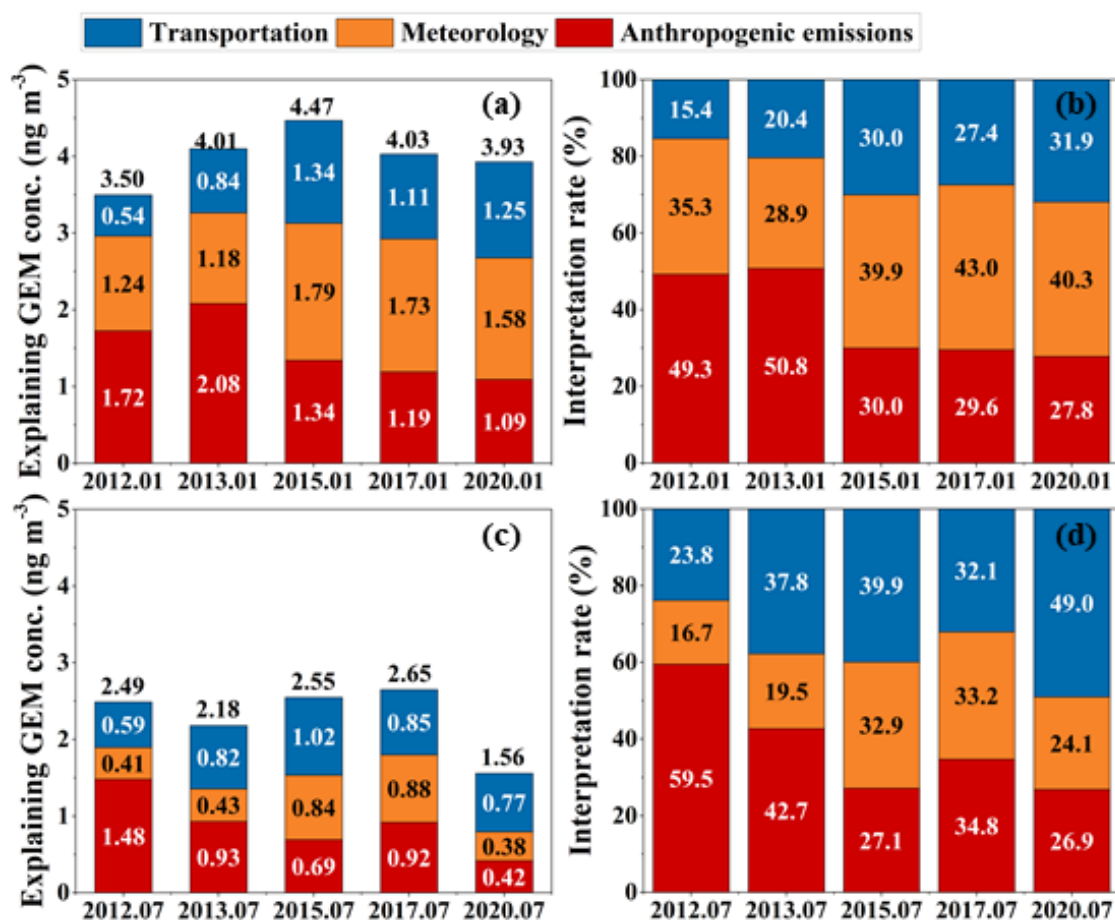
Figure 7. The explaining concentration (ng m^{-3}) (a, c) and interpretation rate (%) (b, d) of the three factors to the variation of GEM concentrations during the study years.

Meteorology was another important factor which explained, on average, $31.4 \pm 9.0\%$ to the variation of GEM concentrations during the whole study period. The inter-annual interpretation rate of meteorology largely varied from 28.9% to 43.0% in January and from 16.7% to 33.2% in July. The largest part of GEM concentrations explained by meteorological factor occurred in January 2015 and July 2017, which were 1.79 ng m^{-3} and 0.88 ng m^{-3}, respectively. The meteorological factor was represented by RH, T and BLH interaction, which influenced GEM variations by several pathways. One is that the meteorological factor drives the Hg chemical transformation (Ariya et al., 2015). In this study, GEM concentrations linearly increased with the increasing RH (Fig.8c). The raise in RH might enhance the liquid phase reduction of process that convert reactive Hg to GEM (Horowitz et al., 2017; Saiz-Lopez et al., 2018; Huang et al., 2019). Another important role is that the meteorological factor is highly related to the Hg emissions from natural surfaces. According to Fig. 8e, f, GEM concentrations increased with the raise of temperature in January, possibly because the increase of temperature would promote the Hg

428 emissions from natural surface (Horowitz et al., 2017; Qin et al., 2019). The meteorological factor also

429 affects the physical state of the atmosphere. A higher BLH likely indicated good diffusion conditions

430 and was more conducive to the reduction of GEM concentrations (Fig. 8g, h). A case in January 18 - 28,

431 2013 shown that the daily GEM concentrations increased with the increase of T and RH as well as the

432 decrease of BLH (Fig. S8). The case also implies that increased temperature likely accelerating natural

433 surface emissions and high RH being favorable for the liquid phase reduction of reactive Hg to GEM

434 contributed to GEM in the atmosphere.
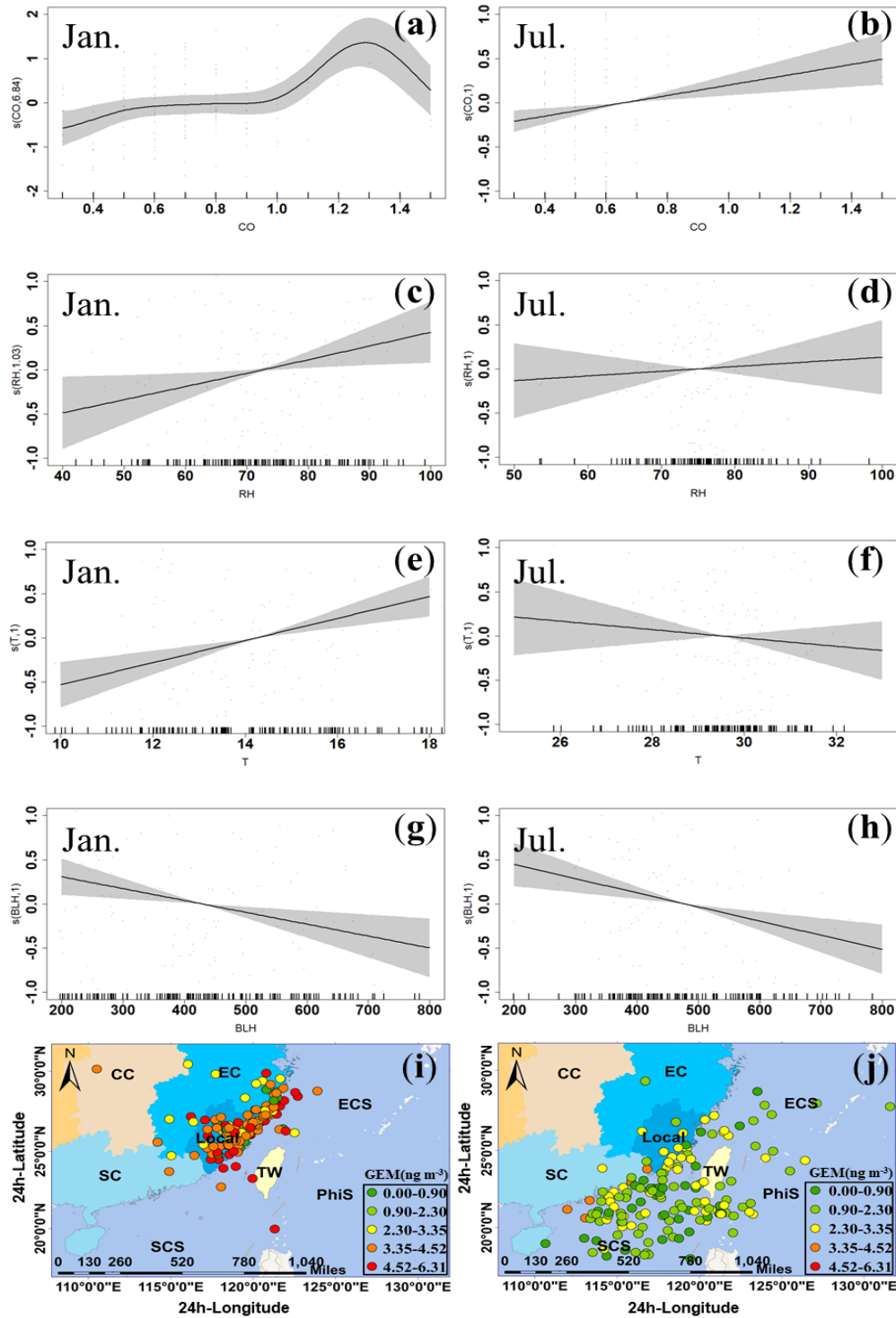
Figure 8. Spline of GEM to the chosen variables, (a, b) CO (mg m^{-3}) in January and July, (c, d) RH (%) in January and July, (e, f) Temperature (°C) in January and July, (g, h) BLH (m) in January and July, (i, j) 24h-Longtitude and 24h-Latitude in January and July. The grey background around the line is 95% confidence bounds for the response. The short lines on x axes show the distribution of data points. The number in the bracket of ordinate title is the estimated degree of freedom. The colored dots in figure (i, j) represents the interactive influence of 24h backward trajectories latitude and longitude coordinates.

442   Regional transportation explained a comparable proportion of GEM concentrations with the

443   meteorological factor, which made up 30.8 ± 9.9% of total variation during the whole study period.

444   During the period of 2012 – 2020, the interpretation rate of transportation displayed an increasing

445   variation from 15.4% to 31.9% in January and a slightly large variation between 23.8% and 49.0% in

446   July. The endpoint of 24 h backward trajectories and corresponding GEM concentrations are shown in

447   Fig. 8i, j. The high GEM concentrations mostly presented in the areas with 24h-Longtitude of 116° –

448   124°E and 24h-Latitude of 24° – 30°N. This is consistent with the backward trajectory results in section

449   3.3.2 that the main source regions of GEM were Fujian province and East China. The interpretation rate

450   of transportation increased significantly among years, indicating the growing importance of

451   transportation from high Hg emission zone to low emission zone in the background of national

452   anthropogenic emissions reduction.

453   **4 Conclusions**

454   Long-term observation of GEM concentrations along with conventional pollutants and meteorological

455   parameters were conducted in Xiamen city, Southeast China. GEM concentrations showed no distinct

456   variation trends over the period 2012 – 2020. GEM concentrations in January were highest in 2015 (4.47

457   ng m^{-3}) and decreased to 2020 (3.93 ng m^{-3}), while GEM concentrations in July were highest in 2017

458   (2.65 ng m^{-3}) and lowest in 2020 (1.56 ng m^{-3}). The temporal variation of GEM was characterized by

459   higher values in winter than in summer and in nighttime than in daytime, which is consistent with those

460   in most urban cities.

461   Upwind point sources within Xiamen city contributed to the elevated GEM concentrations in the study

462   site. Nevertheless, the inter-annual variation trend of GEM was not consistent with those of local SO_2

463   and NOx emissions, suggesting that anthropogenic emissions might be not the dominant influencing

464   factor for GEM variation. The CWT results showed that the pronounced high GEM concentrations in

465   winter 2015 was a regional phenomenon, which was likely due to a combination of high-level Hg

466   emissions and adverse meteorological conditions.

467   The three factors, anthropogenic emissions, meteorological conditions and transportation, which were

468   represented by CO, (RH, T and BLH) interaction, and (24h-Longtitude, 24h-Latitude) interaction,

469   explained $37.8 \pm 11.9\%$, $31.4 \pm 9.0\%$ and $30.8 \pm 9.9\%$ to the variation of GEM concentrations during the

470   whole study period, respectively. There was a positive relationship of GEM with T and RH, suggesting

471   that the meteorological factor influenced GEM variations by several pathways, possibly by affecting the

472   emissions from natural surface and the liquid phase reduction of reactive Hg to GEM. The interpretation

473   rate of transportation and meteorology on GEM variations displayed an increasing trend. In contrast,

474   anthropogenic emissions showed a decreasing interpretation rate since 2012, indicating the effectiveness

475   of emission mitigation measures in reducing GEM concentrations in the study region.

482

483   **Author contributions.** JS and LX designed this study and analysis the data. YuC, LX, YH, ML, XF,

484   YaC, CY GC, LT, JX and JC were involved in the scientific discussion and offered valuable suggestions

485   for modifications**.** JS and LX wrote the manuscript. YuC and JC helped revise the manuscript. and LY

486   managed finances. All authors reviewed the paper.

487

489

490   **Disclaimer.** Publisher's note. Copernicus Publications remains neutral with regard to jurisdictional

491   claims in published maps and institutional affiliations.

492

498

503   **References**

504   Arctic Monitoring and Assessment Programme and United Nations Environment Programme
505   (AMAP/UNEP): Global mercury assessment 2018 – draft technical background document,
506   AMAP/UNEP, Geneva, Switzerland, 2018.
507   Ariya, P. A., Amyot, M., Dastoor, A., Deeds, D., Feinberg, A., Kos, G., Poulain, A., Ryjkov, A.,
508   Semeniuk, K., Subir, M., and Toyota, K.: Mercury physicochemical and biogeochemical
509   transformation in the atmosphere and at atmospheric interfaces: a review and future directions,
510   Chem Rev, 115, 3760-3802, https://doi.org/10.1021/cr500667e, 2015.
511   Axelrad, D. A., Bellinger, D. C., Ryan, L. M., and Woodruff, T. J.: Dose-response relationship of prenatal
512   mercury exposure and IQ: an integrative analysis of epidemiologic data, Environ Health Perspect,
513   115, 609-615, https://doi.org/10.1289/ehp.9303, 2007.
514   Cai, X. R., Cai, B. F., Zhang, H. R., Chen, L., Zheng, C. Y., Tong, P. F., Lin, H. M., Zhang, Q. R., Liu,
515   M. D., Tong, Y. D., and Wang, X. J.: Establishment of High-Resolution Atmospheric Mercury
516   Emission Inventories for Chinese Cement Plants Based on the Mass Balance Method,
517   Environmental Science & Technology, 54, 13399-13408, https://doi.org/10.1021/acs.est.0c02963,
518   2020.
519   Chen, L., Liu, M., Xu, Z., Fan, R., Tao, J., Chen, D., Zhang, D., Xie, D., and Sun, J.: Variation trends
520   and influencing factors of total gaseous mercury in the Pearl River Delta—A highly industrialised
521   region in South China influenced by seasonal monsoons, Atmospheric Environment, 77, 757-766,
522   https://doi.org/10.1016/j.atmosenv.2013.05.053, 2013.
523   Cheng, I., Zhang, L., Blanchard, P., Dalziel, J., and Tordon, R.: Concentration-weighted trajectory
524   approach to identifying potential sources of speciated atmospheric mercury at an urban coastal site
525   in Nova Scotia, Canada, Atmospheric Chemistry and Physics, 13, 6031-6048,
526   https://doi.org/10.5194/acp-13-6031-2013, 2013.
527   Custodio, D., Ebinghaus, R., Spain, T. G., and Bieser, J.: Source apportionment of atmospheric mercury
528   in the remote marine atmosphere: Mace Head GAW station, Irish western coast, Atmospheric
529   Chemistry and Physics, 20, 7929-7939, https://doi.org/10.5194/acp-20-7929-2020, 2020.
530   Diéguez, M. C., Bencardino, M., García, P. E., D'Amore, F., Castagna, J., De Simone, F., Soto Cárdenas,
531   C., Ribeiro Guevara, S., Pirrone, N., and Sprovieri, F.: A multi-year record of atmospheric mercury
532   species at a background mountain station in Andean Patagonia (Argentina): Temporal trends and
533   meteorological influence, Atmospheric Environment, 214,
534   https://doi.org/10.1016/j.atmosenv.2019.116819, 2019.
535   Duan, L., Wang, X., Wang, D., Duan, Y., Cheng, N., and Xiu, G.: Atmospheric mercury speciation in
536   Shanghai, China, Sci Total Environ, 578, 460-468, https://doi.org/10.1016/j.scitotenv.2016.10.209,
537   2017.
538   UN Environment: Financial Rules for the Minamata Convention on Mercury, United Nations
539   Environment Programme, Geneva, Switzerland,
540   https://www.mercuryconvention.org/en/resources/financial-rules-minamata-convention-mercury,
541   2017.

542 Fang, G. C., Lo, C. T., Cho, M. H., Zhuang, Y. J., Tsai, K. H., Huang, C. Y., and Xiao, Y. F.: Annual
543   ambient atmospheric mercury speciation measurement from Longjing, a rural site in Taiwan,
544   Environ Geochem Health, 39, 901-911, https://doi.org/10.1007/s10653-016-9861-x, 2017.

545 Feng, X., Shang, L., Wang, S., Tang, S., and Zheng, W.: Temporal variation of total gaseous mercury in
546   the air of Guiyang, China, Journal of Geophysical Research: Atmospheres, 109, n/a-n/a,
547   https://doi.org/10.1029/2003jd004159, 2004.

548 Friedli, H. R., Arellano, A. F., Cinnirella, S., and Pirrone, N.: Initial estimates of mercury emissions to
549   the atmosphere from global biomass burning, Environ Sci Technol, 43, 3507-3513,
550   https://doi.org/10.1021/es802703g, 2009.

551 Fu, X., Feng, X., Zhu, W., Wang, S., and Lu, J.: Total gaseous mercury concentrations in ambient air in
552   the eastern slope of Mt. Gongga, South-Eastern fringe of the Tibetan plateau, China, Atmospheric
553   Environment, 42, 970-979, https://doi.org/10.1016/j.atmosenv.2007.10.018, 2008.

554 Fu, X. W., Zhang, H., Yu, B., Wang, X., Lin, C. J., and Feng, X. B.: Observations of atmospheric mercury
555   in China: a critical review, Atmospheric Chemistry and Physics, 15, 9455-9476,
556   https://doi.org/10.5194/acp-15-9455-2015, 2015.

557 Fu, X. W., Feng, X., Liang, P., Deliger, Zhang, H., Ji, J., and Liu, P.: Temporal trend and sources of
558   speciated atmospheric mercury at Waliguan GAW station, Northwestern China, Atmospheric
559   Chemistry and Physics, 12, 1951-1964, https://doi.org/10.5194/acp-12-1951-2012, 2012.

560 Gong, X., Hong, S., and Jaffe, D. A.: Ozone in China: Spatial Distribution and Leading Meteorological
561   Factors Controlling O3 in 16 Chinese Cities, Aerosol and Air Quality Research, 18, 2287-2300,
562   https://doi.org/10.4209/aaqr.2017.10.0368, 2018.

563 Gong, X., Kaulfus, A., Nair, U., and Jaffe, D. A.: Quantifying O3 Impacts in Urban Areas Due to
564   Wildfires Using a Generalized Additive Model, Environ Sci Technol, 51, 13216-13223,
565   https://doi.org/10.1021/acs.est.7b03130, 2017.

566 Hong, Q., Xie, Z., Liu, C., Wang, F., Xie, P., Kang, H., Xu, J., Wang, J., Wu, F., He, P., Mou, F., Fan,
567   S., Dong, Y., Zhan, H., Yu, X., Chi, X., and Liu, J.: Speciated atmospheric mercury on haze and
568   non-haze days in an inland city in China, Atmospheric Chemistry and Physics, 16, 13807-13821,
569   https://doi.org/10.5194/acp-16-13807-2016, 2016.

570 Hong, Y., Chen, J., Deng, J., Tong, L., Xu, L., Niu, Z., Yin, L., Chen, Y., and Hong, Z.: Pattern of
571   atmospheric mercury speciation during episodes of elevated PM2.5 levels in a coastal city in the
572   Yangtze River Delta, China, Environ Pollut, 218, 259-268,
573   https://doi.org/10.1016/j.envpol.2016.06.073, 2016.

574 Horowitz, H. M., Jacob, D. J., Zhang, Y., Dibble, T. S., Slemr, F., Amos, H. M., Schmidt, J. A., Corbitt,
575   E. S., Marais, E. A., and Sunderland, E. M.: A new mechanism for atmospheric mercury redox
576   chemistry: implications for the global mercury budget, Atmospheric Chemistry and Physics, 17,
577   6353-6371, https://doi.org/10.5194/acp-17-6353-2017, 2017.

578 Huang, Q., Chen, J., Huang, W., Reinfelder, J. R., Fu, P., Yuan, S., Wang, Z., Yuan, W., Cai, H., Ren,
579   H., Sun, Y., and He, L.: Diel variation in mercury stable isotope ratios records photoreduction of
580   PM2.5-bound mercury, Atmospheric Chemistry and Physics, 19, 315-325,
581   https://doi.org/10.5194/acp-19-315-2019, 2019.

582 Lee, G.-S., Kim, P.-R., Han, Y.-J., Holsen, T. M., Seo, Y.-S., and Yi, S.-M.: Atmospheric speciated
583   mercury concentrations on an island between China and Korea: sources and transport pathways,

Atmospheric Chemistry and Physics, 16, 4119-4133, https://doi.org/10.5194/acp-16-4119-2016, 2016.

Lee, S.-H., Lee, J.-I., Kim, P.-R., Kim, D.-Y., Jeon, J.-W., and Han, Y.-J.: Factors influencing concentrations of atmospheric speciated mercury measured at the farthest island West of South Korea, Atmospheric Environment, 213, 239-249, https://doi.org/10.1016/j.atmosenv.2019.05.063, 2019.

Li, K., Jacob, D. J., Liao, H., Shen, L., Zhang, Q., and Bates, K. H.: Anthropogenic drivers of 2013-2017 trends in summer surface ozone in China, Proc Natl Acad Sci U S A, 116, 422-427, https://doi.org/10.1073/pnas.1812168116, 2019.

Liu, C., Fu, X., Zhang, H., Ming, L., Xu, H., Zhang, L., and Feng, X.: Sources and outflows of atmospheric mercury at Mt. Changbai, northeastern China, Sci Total Environ, 663, 275-284, https://doi.org/10.1016/j.scitotenv.2019.01.332, 2019.

Liu, K., Wang, S., Wu, Q., Wang, L., Ma, Q., Zhang, L., Li, G., Tian, H., Duan, L., and Hao, J.: A Highly Resolved Mercury Emission Inventory of Chinese Coal-Fired Power Plants, Environmental Science & Technology, 52, 2400-2408, https://doi.org/10.1021/acs.est.7b06209, 2018.

Liu, K., Wu, Q., Wang, L., Wang, S., Liu, T., Ding, D., Tang, Y., Li, G., Tian, H., Duan, L., Wang, X., Fu, X., Feng, X., and Hao, J.: Measure-Specific Effectiveness of Air Pollution Control on China's Atmospheric Mercury Concentration and Deposition during 2013-2017, Environ Sci Technol, 53, 8938-8946, https://doi.org/10.1021/acs.est.9b02428, 2019.

Liu, M., Chen, L., Xie, D., Sun, J., He, Q., Cai, L., Gao, Z., and Zhang, Y.: Monsoon-driven transport of atmospheric mercury to the South China Sea from the Chinese mainland and Southeast Asia-Observation of gaseous elemental mercury at a background station in South China, Environmental Science and Pollution Research, 23, 21631-21640, https://doi.org/10.1007/s11356-016-7432-4, 2016.

Marumoto, K., Hayashi, M., and Takami, A.: Atmospheric mercury concentrations at two sites in the Kyushu Islands, Japan, and evidence of long-range transport from East Asia, Atmospheric Environment, 117, 147-155, https://doi.org/10.1016/j.atmosenv.2015.07.019, 2015.

Mason, R.: Mercury emissions from natural sources and their importance in the global mercury cycle, Chapter 7. Interim Report of the UNEP Global Partnership on Atmospheric Mercury Transport and Fate Research 2008.

Nguyen, L. S. P., Nguyen, K. T., Griffith, S. M., Sheu, G. R., Yen, M. C., Chang, S. C., and Lin, N. H.: Multiscale Temporal Variations of Atmospheric Mercury Distinguished by the Hilbert-Huang Transform Analysis Reveals Multiple El Nino-Southern Oscillation Links, Environ Sci Technol, 56, 1423-1432, https://doi.org/10.1021/acs.est.1c03819, 2022.

Qin, X., Wang, X., Shi, Y., Yu, G., Zhao, N., Lin, Y., Fu, Q., Wang, D., Xie, Z., Deng, C., and Huang, K.: Characteristics of atmospheric mercury in a suburban area of east China: sources, formation mechanisms, and regional transport, Atmospheric Chemistry and Physics, 19, 5923-5940, https://doi.org/10.5194/acp-19-5923-2019, 2019.

Qin, X., Zhang, L., Wang, G., Wang, X., Fu, Q., Xu, J., Li, H., Chen, J., Zhao, Q., Lin, Y., Huo, J., Wang, F., Huang, K., and Deng, C.: Assessing contributions of natural surface and anthropogenic emissions to atmospheric mercury in a fast-developing region of eastern China from 2015 to 2018,

Atmospheric Chemistry and Physics, 20, 10985-10996, https://doi.org/10.5194/acp-20-10985-2020, 2020.

Rallo, M., Lopez-Anton, M. A., Contreras, M. L., and Maroto-Valer, M. M.: Mercury policy and regulations for coal-fired power plants, Environ Sci Pollut Res Int, 19, 1084-1096, https://doi.org/10.1007/s11356-011-0658-2, 2012.

Roman, H. A., Walsh, T. L., Coull, B. A., Dewailly, E., Guallar, E., Hattis, D., Marien, K., Schwartz, J., Stern, A. H., Virtanen, J. K., and Rice, G.: Evaluation of the cardiovascular effects of methylmercury exposures: current evidence supports development of a dose-response function for regulatory benefits analysis, Environ Health Perspect, 119, 607-614, https://doi.org/10.1289/ehp.1003012, 2011.

Saiz-Lopez, A., Sitkiewicz, S. P., Roca-Sanjuan, D., Oliva-Enrich, J. M., Davalos, J. Z., Notario, R., Jiskra, M., Xu, Y., Wang, F., Thackray, C. P., Sunderland, E. M., Jacob, D. J., Travnikov, O., Cuevas, C. A., Acuna, A. U., Rivero, D., Plane, J. M. C., Kinnison, D. E., and Sonke, J. E.: Photoreduction of gaseous oxidized mercury changes global atmospheric mercury speciation, transport and deposition, Nat Commun, 9, 4796, https://doi.org/10.1038/s41467-018-07075-3, 2018.

Schroeder, W. H. and Munthe, J.: Atmospheric mercury—An overview, Atmospheric Environment, 32, 809-822, https://doi.org/10.1016/s1352-2310(97)00293-8, 1998.

Sheu, G.-R., Phu Nguyen, L. S., Truong, M. T., and Lin, D.-W.: Characteristics of atmospheric mercury at a suburban site in northern Taiwan and influence of trans-boundary haze events, Atmospheric Environment, 214, https://doi.org/10.1016/j.atmosenv.2019.116827, 2019.

Sheu, G.-R., Lin, N.-H., Lee, C.-T., Wang, J.-L., Chuang, M.-T., Wang, S.-H., Chi, K. H., and Ou-Yang, C.-F.: Distribution of atmospheric mercury in northern Southeast Asia and South China Sea during Dongsha Experiment, Atmospheric Environment, 78, 174-183, https://doi.org/10.1016/j.atmosenv.2012.07.002, 2013.

Shi, J., Chen, Y., Xu, L., Hong, Y., Li, M., Fan, X., Yin, L., Chen, Y., Yang, C., Chen, G., Liu, T., Ji, X., and Chen, J.: Measurement report: Atmospheric mercury in a coastal city of Southeast China: inter-annual variations and influencing factors, Zenodo [data set], https://doi.org/10.5281/zenodo.6573605, 2022.

Slemr, F., Martin, L., Labuschagne, C., Mkololo, T., Angot, H., Magand, O., Dommergue, A., Garat, P., Ramonet, M., and Bieser, J.: Atmospheric mercury in the Southern Hemisphere – Part 1: Trend and inter-annual variations in atmospheric mercury at Cape Point, South Africa, in 2007–2017, and on Amsterdam Island in 2012–2017, Atmospheric Chemistry and Physics, 20, 7683-7692, https://doi.org/10.5194/acp-20-7683-2020, 2020.

Sprovieri, F., Pirrone, N., Bencardino, M., D'Amore, F., Carbone, F., Cinnirella, S., Mannarino, V., Landis, M., Ebinghaus, R., Weigelt, A., Brunke, E.-G., Labuschagne, C., Martin, L., Munthe, J., Wangberg, I., Artaxo, P., Morais, F., Jorge Barbosa, H. d. M., Brito, J., Cairns, W., Barbante, C., del Carmen Dieguez, M., Elizabeth Garcia, P., Dommergue, A., Angot, H., Magand, O., Skov, H., Horvat, M., Kotnik, J., Read, K. A., Neves, L. M., Gawlik, B. M., Sena, F., Mashyanov, N., Obolkin, V., Wip, D., Bin Feng, X., Zhang, H., Fu, X., Ramachandran, R., Cossa, D., Knoery, J., Maruszczak, N., Nerentorp, M., and Norstrom, C.: Atmospheric mercury concentrations observed at ground-based monitoring sites globally distributed in the framework of the GMOS network, Atmospheric Chemistry and Physics, 16, 11915-11935, https://doi.org/10.5194/acp-16-11915-2016, 2016.

Tang, Y., Wang, S., Wu, Q., Liu, K., Wang, L., Li, S., Gao, W., Zhang, L., Zheng, H., Li, Z., and Hao, J.: Recent decrease trend of atmospheric mercury concentrations in East China: the influence of anthropogenic emissions, Atmospheric Chemistry and Physics, 18, 8279-8291, https://doi.org/10.5194/acp-18-8279-2018, 2018.

Wang, C., Wang, Z., and Zhang, X.: Two years measurement of speciated atmospheric mercury in a typical area of the north coast of China: Sources, temporal variations, and influence of regional and long-range transport, Atmospheric Environment, 228, https://doi.org/10.1016/j.atmosenv.2019.117235, 2020.

Wang, C., Wang, Z., and Zhang, X.: Speciated atmospheric mercury during haze and non-haze periods in winter at an urban site in Beijing, China: Pollution characteristics, sources, and causes analyses, Atmospheric Research, 247, https://doi.org/10.1016/j.atmosres.2020.105209, 2021.

Wood, S. N. and Augustin, N. H.: GAMs with integrated model selection using penalized regression splines and applications to environmental modelling, Ecol Model, 157, 157-177, https://doi.org/10.1016/S0304-3800(02)00193-X, 2002.

Wu, Q., Tang, Y., Wang, S., Li, L., Deng, K., Tang, G., Liu, K., Ding, D., and Zhang, H.: Developing a statistical model to explain the observed decline of atmospheric mercury, Atmospheric Environment, 243, https://doi.org/10.1016/j.atmosenv.2020.117868, 2020.

Wu, Q. R., Wang, S. X., Li, G. L., Liang, S., Lin, C. J., Wang, Y. F., Cai, S. Y., Liu, K. Y., and Hao, J. M.: Temporal Trend and Spatial Distribution of Speciated Atmospheric Mercury Emissions in China During 1978-2014, Environmental Science & Technology, 50, 13428-13435, https://doi.org/10.1021/acs.est.6b04308, 2016.

Wu, Q. R., Tang, Y., Wang, L., Wang, S. X., Han, D. M., Ouyang, D. W., Jiang, Y. Q., Xu, P., Xue, Z. G., and Hu, J. N.: Impact of emission reductions and meteorology changes on atmospheric mercury concentrations during the COVID-19 lockdown, Science of the Total Environment, 750, 7, https://doi.org/10.1016/j.scitotenv.2020.142323, 2021.

Wu, Y., Wang, S., Streets, D. G., Hao, J., Chan, M., and Jiang, J.: Trends in anthropogenic mercury emissions in China from 1995 to 2003, Environ Sci Technol, 40, 5312-5318, https://doi.org/10.1021/es060406x, 2006.

Xu, L., Chen, J., Yang, L., Niu, Z., Tong, L., Yin, L., and Chen, Y.: Characteristics and sources of atmospheric mercury speciation in a coastal city, Xiamen, China, Chemosphere, 119, 530-539, https://doi.org/10.1016/j.chemosphere.2014.07.024, 2015.

Yi, H., Tong, L., Lin, J.-m., Cai, Q.-l., Wang, K.-q., Dai, X.-r., Li, J.-r., Chen, J.-s., and Xiao, H.: Temporal variation and long–range transport of gaseous elemental mercury (GEM) over a coastal site of East China, Atmospheric Research, 233, https://doi.org/10.1016/j.atmosres.2019.104699, 2020.

Yin, X., Kang, S., de Foy, B., Ma, Y., Tong, Y., Zhang, W., Wang, X., Zhang, G., and Zhang, Q.: Multi-year monitoring of atmospheric total gaseous mercury at a remote high-altitude site (Nam Co, 4730 m a.s.l.) in the inland Tibetan Plateau region, Atmospheric Chemistry and Physics, 18, 10557-10574, https://doi.org/10.5194/acp-18-10557-2018, 2018.

Yin, X., Zhou, W., Kang, S., de Foy, B., Yu, Y., Xie, J., Sun, S., Wu, K., and Zhang, Q.: Latest observations of total gaseous mercury in a megacity (Lanzhou) in northwest China, Sci Total Environ, 720, 137494, https://doi.org/10.1016/j.scitotenv.2020.137494, 2020.

709   Yu, B., Wang, X., Lin, C. J., Fu, X., Zhang, H., Shang, L., and Feng, X.: Characteristics and potential
710   sources of atmospheric mercury at a subtropical near-coastal site in East China, Journal of
711   Geophysical Research: Atmospheres, 120, 8563-8574, https://doi.org/10.1002/2015jd023425, 2015.
712   Yuan, C. S., Jhang, Y. M., Ie, I. R., Lee, C. E., Fang, G. C., and Luo, J. J.: Exploratory investigation on
713   spatiotemporal variation and source identification of atmospheric speciated mercury surrounding
714   the   Taiwan   Strait,   Atmospheric   Pollution   Research,   12,   54-64,
715   https://doi.org/10.1016/j.apr.2021.01.015, 2021.
716   Zhang, H., Fu, X., Lin, C.-J., Shang, L., Zhang, Y., Feng, X., and Lin, C.: Monsoon-facilitated
717   characteristics and transport of atmospheric mercury at a high-altitude background site in
718   southwestern   China,   Atmospheric   Chemistry   and   Physics,   16,   13131-13148,
719   https://doi.org/10.5194/acp-16-13131-2016, 2016.
720   Zhang, L., Wang, S. X., Wang, L., and Hao, J. M.: Atmospheric mercury concentration and chemical
721   speciation at a rural site in Beijing, China: implications of mercury emission sources, Atmospheric
722   Chemistry and Physics, 13, 10505-10516, https://doi.org/10.5194/acp-13-10505-2013, 2013.
723   Zhang, L., Zhou, P., Zhong, H., Zhao, Y., Dai, L., Wang, Q. g., Xi, M., Lu, Y., and Wang, Y.: Quantifying
724   the impacts of anthropogenic and natural perturbations on gaseous elemental mercury (GEM) at a
725   suburban site in eastern China using generalized additive models, Atmospheric Environment, 247,
726   https://doi.org/10.1016/j.atmosenv.2020.118181, 2021.
727   Zhang, L., Wang, S., Wang, L., Wu, Y., Duan, L., Wu, Q., Wang, F., Yang, M., Yang, H., Hao, J., and
728   Liu, X.: Updated Emission Inventories for Speciated Atmospheric Mercury from Anthropogenic
729   Sources   in   China,   Environmental   Science   &   Technology,   49,   3185-3194,
730   https://doi.org/10.1021/es504840m, 2015.
731   Zhang, Y., Jacob, D. J., Horowitz, H. M., Chen, L., Amos, H. M., Krabbenhoft, D. P., Slemr, F., St Louis,
732   V. L., and Sunderland, E. M.: Observed decrease in atmospheric mercury explained by global
733   decline in anthropogenic emissions, Proc Natl Acad Sci U S A, 113, 526-531,
734   https://doi.org/10.1073/pnas.1516312113, 2016.
735   Zhu, J., Wang, T., Talbot, R., Mao, H., Hall, C. B., Yang, X., Fu, C., Zhuang, B., Li, S., Han, Y., and
736   Huang, X.: Characteristics of atmospheric Total Gaseous Mercury (TGM) observed in urban
737   Nanjing,   China,   Atmospheric   Chemistry   and   Physics,   12,   12103-12118,
738   https://doi.org/10.5194/acp-12-12103-2012, 2012.